ORIGINAL ARTICLE

Comprehensive Analysis of Fibroblast Activation Protein Expression in Interstitial Lung Diseases

Penghui Yang[1]*, Qun Luo[1]*, Xinlu Wang[2]*, Qi Fang[2]*, Zhenli Fu[1]*, Jia Li[1]*, Yunxin Lai[1]*, Xiaobo Chen[1]*, Xin Xu[3]*, Xiaomin Peng[1]*, Kongzhen Hu[4]*, Xiaowei Nie[5], Shaoyu Liu[2], Jinhe Zhang[6], Junqi Li[7], Chenyou Shen[5], Yingying Gu[8], Jianping Liu[1], Jingyu Chen[5], Nanshan Zhong[1], and Jin Su[1,7]

[3]Department of Thoracic Surgery/Oncology, State Key Laboratory, and National Clinical Research Center for Respiratory Disease, [1]State Key Laboratory of Respiratory Disease, National Clinical Research Center for Respiratory Disease, Guangzhou Institute of Respiratory Health, [2]Department of Nuclear Medicine, and [8]Respiratory Pathology Center, Guangzhou Institute of Respiratory Health, The First Affiliated Hospital of Guangzhou Medical University, Guangzhou, Guangdong, China; [4]Department of Nuclear Medicine, Nanfang Hospital, Southern Medical University, Guangzhou, Guangdong, China; [5]Jiangsu Key Laboratory of Organ Transplantation, Wuxi People's Hospital, Nanjing Medical University, Wuxi, China; [6]Department of Nuclear Medicine, General Hospital of Southern Theatre Command of People's Liberation Army of China, Guangzhou, China; and [7]Shenzhen International Institute for Biomedical Research, Shenzhen, Guangdong, China

Abstract

Rationale: Sustained activation of lung fibroblasts and the resulting oversynthesis of the extracellular matrix are detrimental events for patients with interstitial lung diseases (ILDs). Lung biopsy is a primary evaluation technique for the fibrotic status of ILDs, and is also a major risk factor for triggering acute deterioration. Fibroblast activation protein (FAP) is a long-known surface biomarker of activated fibroblasts, but its expression pattern and diagnostic implications in ILDs are poorly defined.

Objectives: The present study aims to comprehensively investigate whether the expression intensity of FAP could be used as a potential readout to estimate or measure the amounts of activated fibroblasts in ILD lungs quantitatively.

Methods: FAP expression in human primary lung fibroblasts as well as in clinical lung specimens was first tested using multiple experimental methods, including real-time quantitative PCR (qPCR), Western blot, immunofluorescence staining, deep learning measurement of whole slide immunohistochemistry, as well as single-cell sequencing. In addition, FAP-targeted positron emission tomography/computed tomography imaging PET/CT

was applied to various types of patients with ILD, and the correlation between the uptake of FAP tracer and pulmonary function parameters was analyzed.

Measurements and Main Results: Here, it was revealed, for the first time, FAP expression was upregulated significantly in the early phase of lung fibroblast activation event in response to a low dose of profibrotic cytokine. Single-cell sequencing data further indicate that nearly all FAP-positive cells in ILD lungs were collagen-producing fibroblasts. Immunohistochemical analysis validated that FAP expression level was closely correlated with the abundance of fibroblastic foci on human lung biopsy sections from patients with ILDs. We found that the total standard uptake value (SUV) of FAP inhibitor (FAPI) PET (SUVtotal) was significantly related to lung function decline in patients with ILD.

Conclusions: Our results strongly support that *in vitro* and *in vivo* detection of FAP can assess the profibrotic activity of ILDs, which may aid in early diagnosis and the selection of an appropriate therapeutic window.

Keywords: fibroblast activation protein; interstitial lung diseases; idiopathic pulmonary fibrosis; positron emission tomography/computed tomography

*These authors contributed equally to this work.

At a Glance Commentary

Scientific Knowledge on the Subject: A noninvasive technique of evaluating the active fibrosis of interstitial lung diseases has been lacking, leading to the late diagnosis of the disease or "blind" prescription of antifibrotic drugs.

What This Study Adds to the Field: Our preclinical and clinical data demonstrate that fibroblast activation protein is a highly specific biomarker of active fibrosis in ILDs and that FAP-targeted PET imaging can be used to predict disease progression.

Fibrosis, a process of excessive accumulation of extracellular matrix (ECM) in response to repeated or chronic injury, can occur in virtually any solid organ and is estimated to contribute to 45% of human deaths from all causes (1, 2). During the past two decades, most efforts toward developing antifibrosis strategies have been paid to a unique indication termed idiopathic pulmonary fibrosis (IPF) because it represents the most lethal form of pulmonary fibrosis (3). The term "idiopathic" means "undetermined or unknown etiology." It is important to understand that IPF, affecting approximately 5 million people worldwide, is one of many forms of interstitial lung diseases (ILDs) and accounts for 20–30% of all ILD cases (3–5). Commonly identified causes for ILDs include occupational/environmental exposures and connective tissue disease.

Regardless of any etiologies, all ILDs share two histological characteristics: variable degrees of inflammation and fibrosis (6). High-resolution computed tomography (HRCT) imaging of the thorax, albeit now acting as a first-line diagnostic tool for ILDs, confirms fibrosis only when typical scarring tissues are formed, leading to delayed

diagnosis. Histopathological examination of the surgical lung biopsy specimens is the current gold standard for the recognition of clinically and radiologically unclassifiable ILDs (7). However, the clinical application of this invasive technique has been limited by relative complexity, cost, and risk of acute deterioration (8). The above diagnostic dilemmas in ILD highlight the need to validate those molecular markers that can be detected with noninvasive *in vivo* approaches.

Fibroblast activation protein (FAP), a 97-kD type II transmembrane serine protease with an extremely long extracellular domain, is known to be not expressed in normal fibroblasts or malignant epithelial cells (9, 10) but highly expressed by the reactive stromal fibroblasts in multiple diseases involving extracellular matrix remodelings, such as cancer (11–13), arthritis (14, 15), fibrosis (16, 17), and atherosclerosis (18). The majority of recent FAP-related publications were predominantly focused on two fields of interest, targeted therapy and molecular imaging. Recently, two studies detailed the ability of engineered T cells expressing FAP antibodies to attenuate cardiac fibrosis through depleting those FAP-expressing myofibroblasts (17, 19). FAP-specific inhibitors (FAPIs), initially developed as anticancer drugs (20, 21), were recently advanced into radiopharmaceuticals and quickly and widely applied in the *in vivo* positron emission tomography (PET) imaging of activated fibroblasts under several human pathological conditions, such as cancer (22), IgG4-related disease (IgG4-RD) (23), and arthritis (24). Notably, the FAPI-PET/CT imaging exhibited a high signal-to-background ratio even 10 minutes after tracer injection because of its several advantages, such as rapid and high uptake by pathological tissues, very low accumulation in normal tissues, as well as rapid clearance from the kidney (15 min after injection) (25).

Two aspects of evidence have been presented regarding the link between FAP and ILDs. An early preliminary study of eight IPF lung tissue sections reported that FAP expression was located within the ongoing fibrosis areas of IPF lungs rather

than the adjacent normal lung tissues (16). In experimental pulmonary fibrosis, the contribution of FAP to the disease outcome seemed to rely highly on the initiating insult for model induction (26, 27). Therefore, the detailed expression pattern of FAP during lung fibroblast activation and in various types of ILD remains unclear. Hence, the present study investigates these issues through several experimental approaches with quantitative traits, including real-time quantitative PCR (qPCR), Western blot, deep learning measurement of whole slide immunohistochemistry (IHC), single-cell sequencing, and FAP-targeted PET/CT.

Study Design

A major goal of this study is to validate the expression patterns of FAP in various subtypes of ILDs. Western blot, qPCR, IHC, immunofluorescence, single-cell sequencing, and PET/CT imaging were used in our study. Each *in vitro* experiment was performed at least twice to eliminate assay-specific artifacts. The complementary DNA (cDNA) sequence encoding the extracellular segment of human FAP protein was ligated with a lentiviral vector, and the recombinant construct was then transfected into 293T cells to verify the specificity of a commercial antibody against FAP (#66562, Cell Signaling). Parental or FAP-overexpressing A549 cells were transplanted into nude mice, and the corresponding xenografts were then subjected to PET/CT imaging with ^{68}Ga-FAPI-04 as previously described (28). The medical certificates were given by professional and experienced ILD physicians and pathologists in the First Affiliated Hospital of Guangzhou Medical University for all clinical specimens. In the immunohistochemical study, artificial intelligence software was applied to quantitatively calculate the positive staining signals. For PET data analysis, the total uptake volume of the radioactive probe was used to reflect the FAP expression intensity in the whole lung.

Correspondence and requests for reprints should be addressed to Jin Su, Ph.D., State Key Laboratory of Respiratory Disease of Guangzhou Medical University, 195 Dongfengxi Road, Yuexiu District, Guangzhou 510182, China. E-mail: sujin@gird.cn.

This article has a related editorial.

This article has an online supplement, which is accessible from this issue's table of contents at www.atsjournals.org.

Methods

Human Lung Tissues

The study on clinical samples was approved by the Ethics Committee of the First Affiliated Hospital of Guangzhou Medical University. All the ILD specimens were obtained from either lung transplantation surgery or lung biopsy. The classification of ILD was made by each subject's primary pulmonologist according to American Thoracic Society/European Respiratory Society guidelines. The healthy lung tissue samples were from organ donors diagnosed with brain death. Before collection, the written consents for tissue harvesting were obtained from each patient or family member.

Isolation of Human Primary Lung Fibroblasts and Treatment with Transforming Growth Factor β (TGF-β)

Human primary lung fibroblasts (hPLFs) were separated and cultured as follows: briefly, the lung tissues from healthy donors were cut into small pieces and then immersed in Dulbecco's modified Eagle's medium (GIBICO, Life Technologies Corporation) containing collagenase II (2 mg/ml), trypsin (2.5 mg/ml), DNase I (2 mg/ml), penicillin (100 U/ml), and streptomycin (100 μg/ml) for 12 hours at 37°C followed by Dulbecco's phosphate-buffered saline washing. The cells were collected from the supernatant after removing the remaining tissue lumps by 70 μm cell filters and then maintained in Dulbecco's modified Eagle's medium supplemented with heat-inactivated 10% fetal bovine serum (#10099141, Gibco). High purity of fibroblasts can be obtained after passage over three times; 3×10^5 hPLFs at 50% confluence from a healthy donor were plated in a six-well plate and treated with 10 ng/ml TGF-β for different durations. For the dose-dependent experiment, different concentrations of TGF-β were added to the six-well plate for 48 hours.

Establishment of Pulmonary Fibrosis Animal Model

C57BL/6J mice were obtained from Hunan SJA Laboratory Animal Co., Ltd. All mice were produced and housed in a specific pathogen-free barrier area. All animal procedures were approved by the Animal Care and Use Committee of Guangzhou Medical University. A total of 2.0 mg/kg Bleomycin (BLM, Hisun Pfizer Pharmaceuticals Co., Ltd.) in saline was administered intratracheally to induce lung fibrosis using a 1 ml syringe with a 25G needle with insertions between the cartilaginous rings of the trachea. Mice were killed, and lung tissues were collected after BLM at different durations.

Western Blot Analysis

Western blot experiments were performed as described previously (29). Briefly, cell lysates or lung tissue homogenates were prepared using ice-cold radioimmunoprecipitation assay lysis buffer: 0.05 M Tris-HCl pH 7.4, 0.15 M NaCl, 0.25% deoxycholic acid, 1% NP-40, 1 mM ethylenediamine-tetraacetic acid, and protease inhibitor cocktail. The protein concentrations of the lysates were determined by a commercial Bradford reagent kit (Shanghai Yeasen Biotech Co., Ltd.). Equal amounts of protein (5–10 μg) were separated with Geneshare CFAS anyKD sodium dodecyl sulfate-polyacrylamide gel electrophoresis (Shanxi ZHHC Biotechnology Co., Ltd.) and then transferred to nitrocellulose membranes (Millipore). After blocking with 4% bovine serum albumin (BSA) in Tween 20-Tris-buffered saline, the membranes were incubated with the primary antibodies against the following target proteins: FAP (#66562, Cell Signaling), fibronectin (#ab2413, Abcam), β-actin (#3700, Cell Signaling), and then detected with horseradish peroxidase-conjugated goat anti-rabbit or anti-mouse IgG (#SSA018 and #SSA021, Sino Biological Inc). Specific protein bands were visualized by an enhanced chemiluminescence machine (BLT 6000Plus, Biolight Biotechnology Co., Ltd.) and quantified with Image J software (Ver. 1.51).

Real-time Quantitative PCR (qPCR)

Total tissue or cell RNA was extracted using EZ-press RNA Purification Kit (EZBioscience). cDNA was synthesized using the Super-Script III First-Strand Synthesis System (18080051, Invitrogen). qPCR was conducted on a real-time thermocycler CFX96 (Bio-Rad Laboratories) with $2 \times$ SYBR Green Ndcleic Acid Gel Stains, SYBR Green is a common form qPCR Mix (Yeasen Biotech). The primer sequences used were as follows: FAP: CAAAGGCTGGAGCTAAGAATCC (forward); ACTGCAAACATACTCGTTCATCA (reverse); β-actin: CATGTACGTTGCTATCCAGGC (forward); CTCCTTAATGTCACGCACGAT (reverse). qPCR data indicate the relative mRNA expression level of the target gene, and β-actin was used as an internal reference control.

Immunofluorescence Staining

For immunofluorescent analysis of FAP expression in hPLFs, the cells cultured on a 24-well plate (1.5×10^4 cells/well) were treated with 10 ng/ml (TGF-β) (#10804-H08H, Sino Biological) for different durations and then subjected to fixation with 4% paraformaldehyde for 15 minutes and permeabilization with 0.1% Triton X-100 in phosphate-buffered saline. After blocking with 5% BSA for 1.5 hours at 37°C, the cells were incubated with primary antibody against FAP (#66562, Cell Signaling) at a dilution of 1:50 at 4°C overnight. Goat anti-rabbit IgG labeled with Alexa Fluor 594 (#ab150080, Abcam) was used as the secondary antibody with 1:200 dilution. Nuclei were stained with 1 μg/ml 4,6-diamidino-2-phenylindole (DAPI) (Thermo Fisher, 1 μg/ml). The fluorescence images of the cells were collected using a Leica Dmi8 fluorescence microscope and merged with Adobe Photoshop CC 2019 software.

Single-cell Analysis

Cellranger mkfastq demultiplexes raw base call files generated by Illumina sequencers into FASTQ files. Cellranger 6.0 was used to generate raw counts (using GRCh38 as a reference) for each gene in each cell. Seurat 4.0 was used to preprocess the data, perform quality control, and filter out low-quality cells. We further filtered out the cells with detected genes numbered less than 200 and mitochondria percentage larger than 10%; we also removed the genes detected in less than 50 cells. The doublet was detected and removed by using DoubletFinder. We used a marker gene set from a previous study (30) to annotate the cells. The standard Seurat analysis pipeline was used to normalize the raw counts for each gene in each cell and visualize the gene expression level in each cell.

IHC

The paraffin-embedded lung tissue sections (4 μm) were dewaxed and rehydrated through graded alcohol, followed by antigen retrieval by high-pressure cooking for 2 minutes in 10 mM citrate acid. The endogenous peroxidase activity was cleared using 3% H_2O_2 in methanol for 10 minutes. After incubation with 5% BSA for 1 hour, the sections were stained with rabbit anti-human monoclonal antibodies against FAP (#66562,

Cell Signaling) or normal rabbit IgG overnight at 4°C at a dilution of 1:50 and then incubated with biotinylated goat anti-rabbit IgG (Beyotime Biotechnology) at a dilution of 1:200 for 30 minutes at room temperature. All sections were subjected to color development with peroxidase-conjugated avidin/biotin and 3′-3-diaminobenzidine (DAB) substrate (Beyotime Biotechnology), followed by counterstaining with hematoxylin.

Computer-based Artificial Intelligence Analysis of Immunohistochemical Staining Images

DAB-stained slides were fully scanned with the Aperio ScanScope CS2 device (Aperio Technologies) at 20× objective magnification to obtain the whole slide image (WSI). Five areas (1 mm^2 each) on each WSI were randomly selected for further analysis of the IHC staining signals with an open-source tool called Orbit Image Analysis (www.orbit.bio), as described recently (30). Briefly, the IHC analysis model was trained on the basis of a sliding window feature extraction approach, which uses different features as predictors to classify the center pixel label to discriminate regions within the image, such as normal lung alveoli and airways, hematoxylin-stained nucleus, DAB-stained positive signals, and blank parts outside the tissue and within the airways. A training set of representative DAB-stained images were used to train the machine learning model. The IHC analysis model can sensitively recognize the different components within the slides. For measurement of the percentage of FAP-positive areas, each tissue slice was divided into three parts (FAP-positive, FAP-negative, and blank). Then the ratio of the FAP-positive area to the total area without blank was calculated.

PET/CT Imaging for Patients

Patients and radiopharmaceuticals. The PET/CT study on patients with ILD was approved by the ethics committee of the First Affiliated Hospital of Guangzhou Medical University and then registered on the Chinese Clinical Trial Registry (http://www.chictr.org.cn/showproj.aspx?proj=124983) with the ID ChiCTR-IPR-2100045352. All enrolled patients signed written informed consent. The diagnosis information of patients was also retrospectively collected with the approval of the local ethics committee. ^{68}Ga-FAPI-04 was synthesized by experienced technicians working in the department of nuclear

medicine (the First Affiliated Hospital of Guangzhou Medical University) and subjected to use when their purity reached above 95%.

PET/CT imaging. All imaging tests were performed with a Discovery ST PET/CT machine (GE Healthcare). Patients dedicated to ^{68}Ga-FAPI-04 scan can directly be subjected to injection of tracers (0.05–0.15 mCi/kg) without fasting. The CT scan parameters were as follows: voltage, 140 kV; current, 150 mA; pitch, 1.675; time, 20–30 seconds; reconstructed with a slice thickness of 3.75 mm and lung slice thickness of 2.5 mm.

Imaging analysis. The entire lung was manually segmented by two independent, experienced nuclear medicine doctors using the Advantage Workstation (AW 4.7 extension 8, GE Healthcare). The mean standardized uptake value (SUVmean) of mediastinal blood pool activity was set as the absolute threshold value. A region of interest (ROI) was determined by three-dimensional segmentation of those voxels above the predefined threshold, and the total volume of ROI was defined as the total active volume. The SUVtotal of ^{64}Ga-FAPI tracer in each lung was calculated by multiplying the SUVmean of ROI by the total active volume.

Measurement of Serum Concentration of KL-6 (Krebs von den Lungen-6) and Pulmonary Function Test (PFT)

The serum concentration of KL-6 in each patient was measured no more than 10 days before PET/CT test by a commercially available chemiluminescence enzyme immunoassay-based kit (Lumipulse KL-6Eisai, Fujirebio) according to the manufacturer's protocol.

Pulmonary function tests were performed on patients with ILD by the same respiratory lab technicians in the First Affiliated Hospital of Guangzhou Medical University with a MasterScreen PFT system (Jeager) according to the guidelines of the ATS (American Thoracic Society). The first PFT was conducted within 1 month of the PET/CT scan. The time interval between the two PFT measurements was approximately 4–20 months.

Statistical Analysis

Statistical analyses were performed using IBM SPSS (Statistical Product, Service Solutions) Statistics 21 and GraphPad Prism 6 software. In the case of normally distributed data, one-way ANOVA and least significant difference *t* tests were used to

compare groups of more than three. Paired *t* tests were used to compare two samples. For nonnormally distributed data, the nonparametric Kruskal-Wallis test was used. Pearson's correlation coefficients were calculated for the correlation analysis. A two-tailed *P* value of less than 0.05 was considered significant.

Results

FAP Expression Can Be Induced in the Early Phase of Lung Fibroblast Activation

TGF-β represents the most potent profibrotic cytokine and has been well established to induce the transition of lung fibroblasts from a quiescent to an activated phenotype, featuring an increased expression of several key fibrotic marker genes, such as α-SMA (α-smooth muscle actin) and fibronectin (31). The TGF-β induction of FAP was previously examined in both cancer cells and lung fibroblast cell lines (32, 33). Here, the expression of FAP and other fibrosis markers induced by TGF-β at different doses and different time points was detected simultaneously. The specificity of the commercial FAP antibody was first verified by immunoblot of FAP-overexpressing 293T cells (Figure E1 in the online supplement).

Primary human lung fibroblasts from healthy donors were treated with TGF-β for various durations and then subjected to analysis for gene expression of FAP, fibronectin, and α-SMA. The results showed that FAP could be detected as early as 24 hours of TGF-β stimulation, reached its peak at 48 hours, and maintained a stable and high concentration until 72 hours. In sharp contrast, the expression of fibronectin and α-SMA appeared to be significantly upregulated at a relatively late time point (Figures 1A and E2A). The TGF-β–dependent upregulation of FAP at 24 hours of TGF-β treatment was further confirmed by immunofluorescence staining (Figure 1B). In addition, we observed that FAP protein was completely absent in resting lung fibroblasts. Next, we examined the response of these fibrotic markers to various doses of TGF-β and found that FAP can be detected in a lower dose of TGF-β induction than α-SMA and fibronectin (Figures 1C and E2B). Consistent with these findings, we observed an increase in FAP expression in the bleomycin-induced lung fibrosis models

beginning 1 week after injury and maintained a high level until 4 weeks later. However, fibronectin expression was pronounced upregulated 3 weeks after model establishment (Figures 1D and E2C). These data collectively suggest that FAP might be a relatively sensitive surrogate/marker for the early stage of lung fibroblast activation.

Total Abundance of FAP in the Late Stage of ILD Lungs

Although a previous study using immunohistochemical methods documented the rich presence of FAP in IPF lungs (16), quantitative and comparative analysis of its concentration among distinct ILDs has not been performed so far. Herein, we collected human lung tissues of patients with late-stage IPF and patients with silicosis from lung

transplantation surgery and analyzed the FAP expression profile using qPCR and Western blot. Compared with healthy donors, the protein and mRNA concentration of FAP was dramatically increased in four out of eight patients with IPF, and the other four patients with IPF only showed a minor increase. Although we observed a large variation of FAP protein concentrations among 12 patients with silicosis, almost all 12 patients with silicosis had a higher FAP protein concentration than healthy donors (Figures 2A and 2B). In addition, our results showed that the mRNA concentration of FAP in patients with silicosis (non-IPF) was significantly lower than that in patients with IPF (Figure 2C). These data revealed a wide range of FAP expression concentrations in lung tissues of

patients with late-stage ILD, indicating the high heterogeneity of activated fibroblast abundance in different patients.

FAP mRNA Expression in ILD Lungs Is Exclusively Derived from Fibroblasts

To characterize the cell types that express the FAP gene in ILD lungs, we reanalyzed and annotated 89,326 single cells (31,644 cells from 10 nonfibrotic control and 57,682 cells from 20 pulmonary fibrosis lungs) from an elegant study (30). The violin plot, uniform manifold approximation, and projection plot collectively showed that FAP was mostly and exclusively expressed by the clusters of fibroblast origin (91%) (Figures 3A–3C). To further validate that FAP's expression level was correlated with fibroblast activity, we performed a correlation
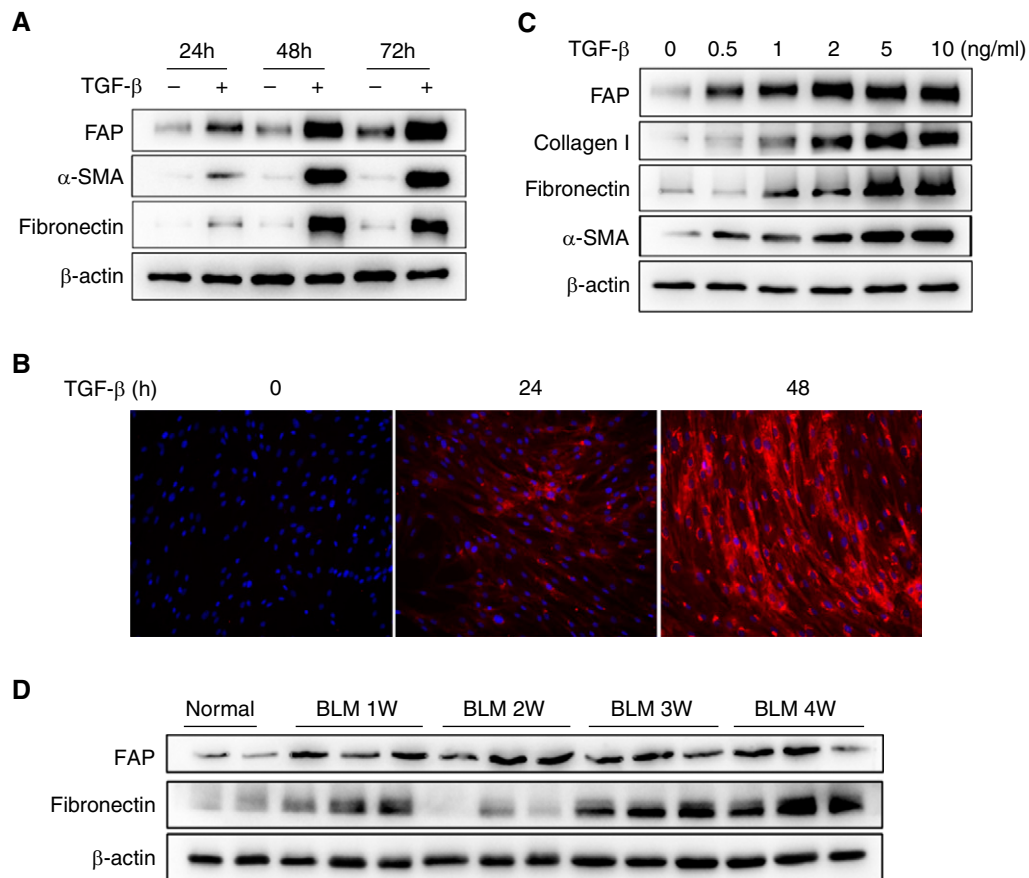

Figure 1. Transforming growth factor β (TGF-β) modulation of fibroblast activation protein expression in human primary lung fibroblasts. (*A*) Human primary lung fibroblasts from healthy donors were treated with TGF-β (10 ng/ml) for the indicated times (24, 48, and 72 h). The corresponding negative control at each time point was set and then subjected to Western blot to analyze the expression of fibroblast activation protein (FAP), fibronectin, and α smooth muscle actin (α-SMA). (*B*) At the same time, immunofluorescence staining was used to detect the expression of FAP at different time points after being treated with TGF-β (10 ng/ml). The red color represents FAP immunoreactive signals, whereas the blue indicates DAPI staining. (*C*) Five concentration gradients (0.5, 1, 2, 5, and 10 ng/ml TGF-β) and negative control (0 ng/ml TGF-β) groups were implemented for 48 hours in a TGF-β dose-dependent experiment. Western blot analysis was used to detect the FAP, fibronectin, collagen I, and α-SMA. (*D*) Expression of FAP in mouse lung tissues at different time points after bleomycin (BLM) model.

analysis between the expression of FAP and classical myofibroblast marker genes: *COL1A1* (collagen I), *ACTA2* (α-SMA), and *FN1* (fibronectin) in single-cell level. Our analysis showed that FAP's expression level was significantly correlated with *ACTA2* ($r = 0.458$; $P < 0.0001$), *FN1* ($r = 0.403$; $P < 0.0001$) and *COL1A1* ($r = 0.230$; $P = 0.0101$) in fibroblast cells (Figure 3D). In addition, we obtained consistent results by performing a similar analysis using another independent small conditional RNAseq (scRNAseq) dataset (GSE136831), which included 28 control subjects (81,522 cells) and 32 IPFs (119,975 cells) (Figure E3). Above all, our single-cell analysis collectively suggests that FAP could be a reliable biomarker for myofibroblasts in ILDs.

FAP Protein Abundance Correlates with the Grades of Fibroblastic Foci in ILDs

To further explore whether the localization of FAP protein in ILD lungs is clinically associated with the abundance of activated fibroblasts, the lung biopsy tissue sections from 33 patients with diverse etiologies for ILDs were subjected to immunohistochemical staining with anti-FAP monoclonal antibody (Figure 4A). The grades of fibroblast foci were assigned to the following three grades according to the pathologist's description: (3) if rich and wide-spread; (2) if observable; and (1) if very few (Table 1). The positive staining areas on WSI were quantified through a recent deep machine-learning algorithm (30). It was demonstrated that the average values of

both fibroblast foci grades and FAP-positive areas in the IPF group ($n = 7$) were significantly higher than those in the non–IPF–ILD group ($n = 26$) (Figures 4B–4D). In addition, these two parameters were well correlated in all patients (Figure 4E) ($r = 0.6056$; $P = 0.0002$). These results suggest that irrespective of etiologies, FAP expression might be a surrogate for the fibrotic status of all types of ILDs.

PET/CT Study with ⁶⁸Ga-FAPI in Various Types of Patients with ILD

To investigate the *in vivo* distribution profile of FAP-positive cells in ILD lungs, FAPI-04, a selective FAP-binding compound, was labeled by nuclide ⁶⁸Ga and then applied in PET/CT imaging of the thorax. The *in vivo*
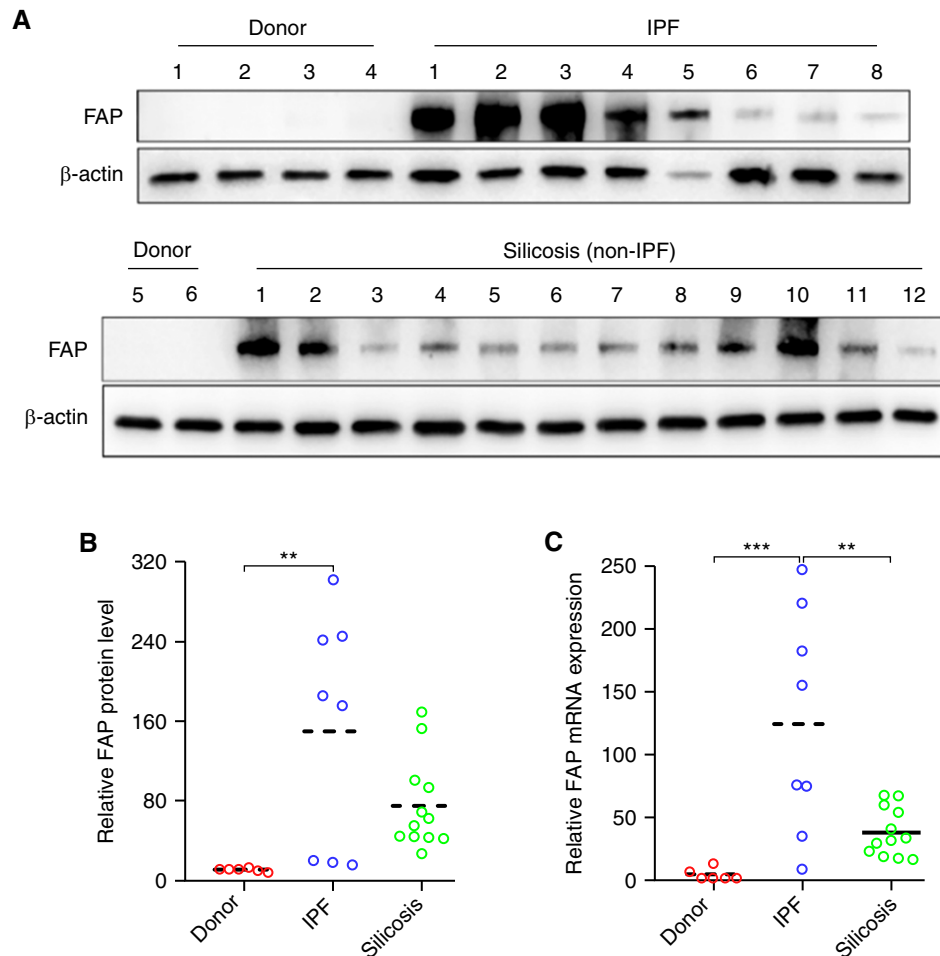

Figure 2. Expression of protein and mRNA of fibroblast activation protein (FAP) in transplanted lung tissue for patients with and without idiopathic pulmonary fibrosis (IPF). (*A* and *B*) The frozen lung tissues from healthy donors ($n = 6$) and patients with IPF ($n = 8$) or non-IPF interstitial lung disease (silicosis, $n = 12$) were used for FAP expression evaluation by Western blot. **$P < 0.01$. (*C*) Real-time PCR analysis of FAP mRNA expression. β-actin was used as an internal reference gene to normalize the expression of FAP. The relative expression of FAP in one healthy donor (1#) was designated as sample control and set at one. The expression folds in other individuals were calculated through comparison to control subjects. The dashed line is a median. **$P < 0.01$ and ***$P < 0.001$.
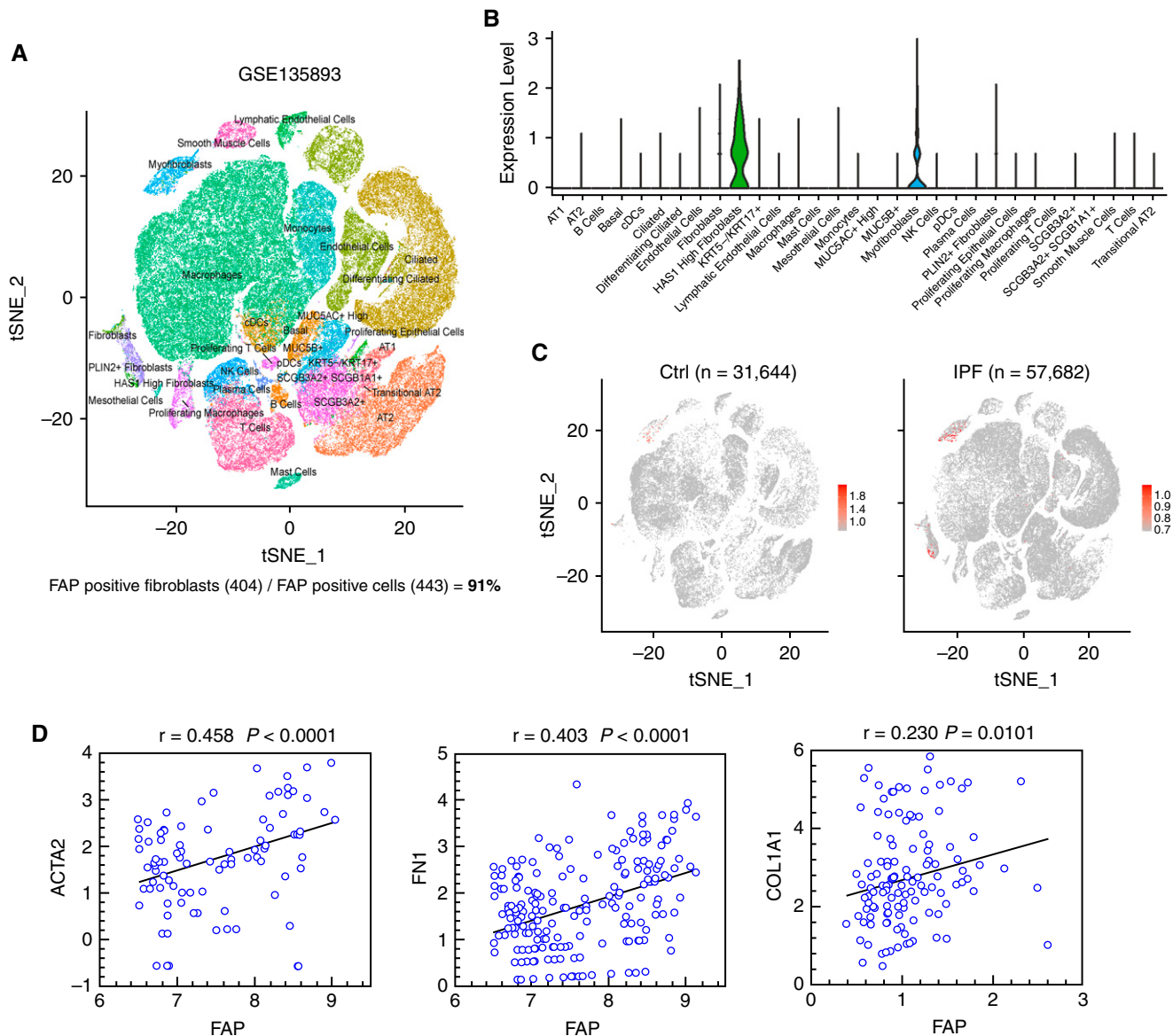
Figure 3. Single-cell analysis reveals the specific expression of fibroblast activation protein (FAP) in fibroblasts from the public data. (*A*) Uniform manifold approximation and projection (UMAP) shows the control and idiopathic pulmonary fibrosis (IPF) single-cell populations from study GSE135893. (*B*) *FAP* expression level in each cell population using single-cell RNA sequencing data from study GSE135893. (*C*) UMAP shows the cells that express *FAP* in healthy donors and patients with IPF from study GSE135893. (*D*) Expression correlation analysis between *FAP* and *ACTA2*, *FN1*, and *COL1A1* (the x-axis and y-axis represent log2 normalized expression level). cDCs = conventional dendritic cells; Ctrl = control; NK = natural killer; tSNE = t-distributed stochastic neighbor embedding.

specificity of ^{68}Ga-FAPI-04 against FAP was verified by observing its uptake in nude mice bearing human FAP cDNA-overexpressing A549 tumors. As expected, ^{68}Ga-FAPI-04 uptake could only be observed in FAP-transduced tumor xenografts rather than in untransduced control subjects (Figures E4A and E4B). Cell-based experiments further indicated that TGF-β treatment of primary human lung fibroblasts significantly increased the cell uptake of ^{18}F-FAPI but had no effect on that of ^{18}F-FDG (Figure E4C).

These results imply that FAP-positive fibroblasts could be specifically labeled by ^{68}Ga-FAPI-04 *in vivo*.

A total of 83 patients with ILD and 8 healthy volunteers were recruited for the PET/CT study with ^{68}Ga-FAPI-04 after providing written informed consent. The clinical characteristics of all diseased participants in our PET/CT study were listed in Table 2, and more than 90% of patients received antifibrotic therapy by pirfenidone. The patients consisted of 20 individuals with

IPF and 63 individuals without IPF, including idiopathic nonspecific interstitial pneumonitis (NSIP, 15 cases), connective tissue disease (CTD, 28 cases), as well as interstitial pneumonia with autoimmune features (IPAF, 20 cases). Representative images of CT and PET/CT for healthy volunteers and patients with ILD were demonstrated in Figure 5A. The distribution pattern of ^{68}Ga-FAPI-04 in the whole lung was reflected by the SUVtotal (Figure 5A, right panel). The calculation data showed
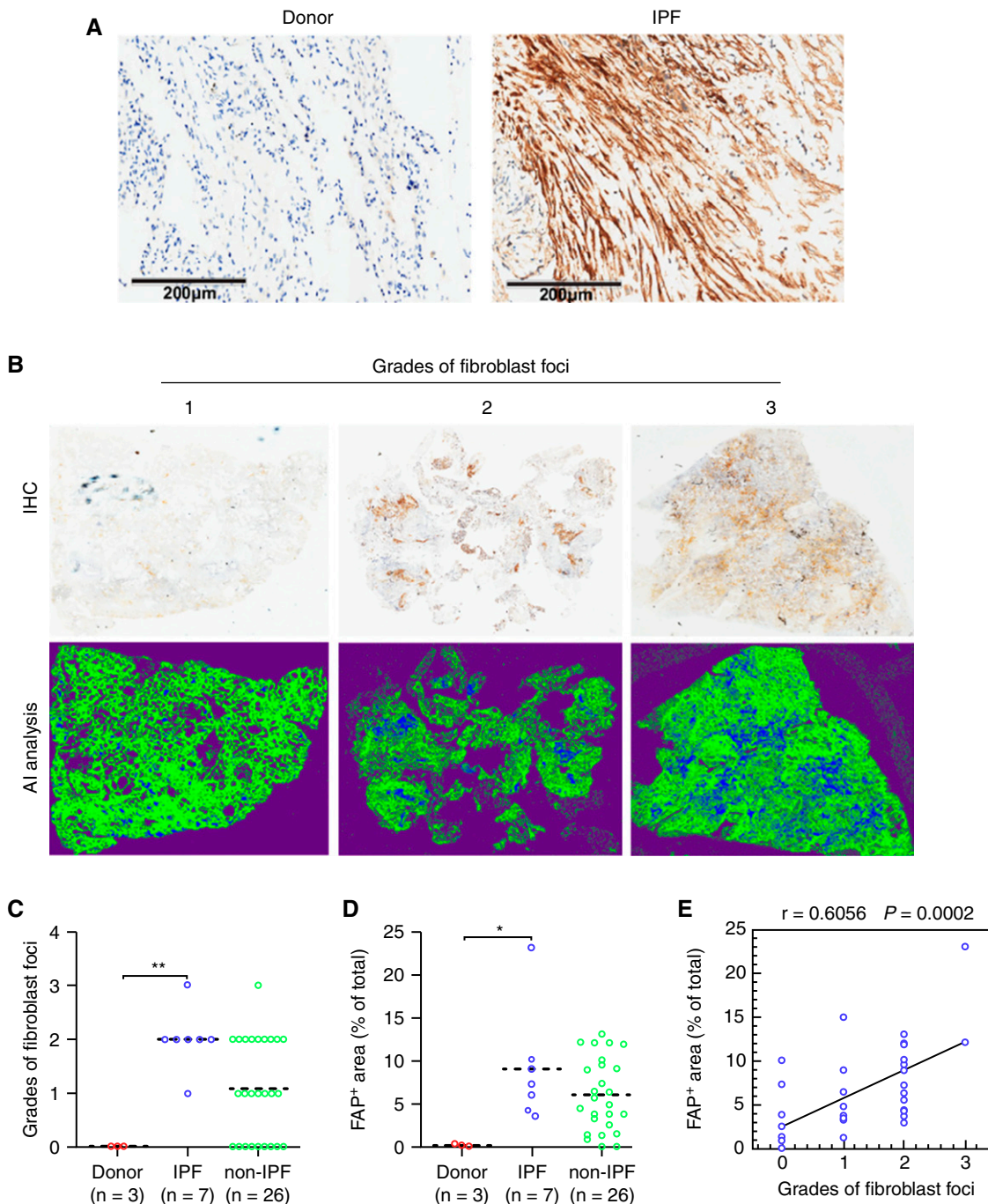
Figure 4. Fibroblast activation protein (FAP) expression in lung biopsies of patients with and without idiopathic pulmonary fibrosis (IPF). The lung biopsy tissue sections of IPF ($n = 7$) and non-IPF interstitial lung disease (ILD) ($n = 26$) were subjected to immunohistochemical staining of FAP. (*A*) Representative higher magnification immunohistochemistry images for FAP expression in donors and patients with IPF. Scale bars, 200 μm. (*B*) Representative immunohistochemistry images for patients with ILD with different grades of fibroblast foci (+, ++, and +++). The *above* columns indicate panorama images of original immunohistochemistry for the whole slide images, and the *below* columns indicate the positive signal extraction (blue) by artificial intelligence analysis. The grades of (*C*) fibroblast foci and (*D*) percentages of FAP-positive areas within the WSI for donors, patients with ILD and IPF, and patients with ILD but without IPF. (*E*) Correlation between the percentages of FAP-positive areas and the grades of fibroblast foci for patients ($n = 33$), including IPF and non-IPF, $r = 0.6056$; $P = 0.0002$, data are shown in correlation plots. The dashed line is a median. $*P < 0.05$ and $**P < 0.01$.

Table 1. Baseline Characteristics of Patients with Definite Diagnosis and Staining Index with Fibroblast Activation Protein

		Non-IPF (n = 26)		
Diagnostic Criteria	IPF (n = 7)	Idiopathic NSIP (n = 7)	ASS (n = 13)	RA (n = 6)
Male sex, n (%)	5 (71.4)	3 (37.5)	4 (30.8)	3 (50)
Age (yr), mean (range)	62.1 (57–70)	47.9 (40–60)	52.8 (34–68)	53.3 (34–61)
Autoantibody, n (%)				
ANA	0	0	10 (76.9)	3 (50)
Anti-Ro-52	0	0	12 (92.3)	2 (33.3)
Anti-Jo-1	0	0	4 (30.8)	0
Anti-PL-12	0	0	4 (30.8)	0
Anti-CCP	0	0	0	4 (66.7)
RF (U/ml), mean (range)	<20	<20	<20	365.8 (22–717)
HRCT type, n (%)				
NSIP	0	7 (100)	9 (69.2)	1 (16.7)
UIP	7 (100)	0	4 (30.8)	5 (83.3)
Fibroblast foci, n (%)				
None	0	4 (57.1)	4 (30.8)	—
Few/little	1 (14.3)	3 (42.9)	4 (30.8)	1 (16.7)
Visible/existent	5 (71.4)	0	4 (30.8)	5 (83.3)
Great amount/broad	1 (14.3)	0	1 (7.7)	—
FAP+ (%), mean (range)	8.6 (3.0–23.1)	4.1 (0.1–15.1)	6.2 (0.1–12.2)	8.3 (3.8–13.1)

Definition of abbreviations: ANA = antinuclear antibody; ASS = antisynthetase syndrome; CCP = cyclic citrullinated peptide; HRCT = high-resolution computed tomography; IPF = idiopathic pulmonary fibrosis; NSIP = nonspecific interstitial pneumonitis; RA = rheumatoid arthritis; RF = rheumatoid factor; UIP = usually interstitial pneumonia.

that patients with IPF did not differ significantly from non-IPF counterparts in the mean SUV (SUVmean) (Figure 5B). The median values of the total SUV (SUVtotal) were much higher in the IPF group than in the non-IPF group, suggesting a diffuse distribution pattern of tracer uptake in IPF (Figure 5C). KL-6 is currently the most reliable serum biomarker reflecting the severity of ILDs (34). Here we found that the patients' concentration of KL-6 in serum (approximately within the 10-day interval from their PET/CT examination) were significantly positively associated with their values of SUVtotal ($r = 0.3453$; $P = 0.0018$) but not with those of SUVmean ($r = 0.0761$; $P = 0.5052$) (Figure 5D).

Next, baseline values of FVC and $D_{L_{CO}}$, the two important prognostic lung function parameters in ILDs (35, 36), were examined 1 month before or after PET/CT test and compared with the patients' PET values. Among the recruited 83 patients with ILD, 32 received the second time of PFT evaluation several months (4–20) after the first test, and hence the changes in lung function in these patients could be obtained (Figure 6A). Consistent with the above data, the values of both the baseline PFT and the PFT changes were not correlated with

Table 2. Characteristics of the Participants in Our Study for Positron Emission Tomography/Computed Tomography

		Non-IPF (n = 63)		
Diagnostic Criteria	IPF (n = 20)	Idiopathic NSIP (n = 15)	CTD (n = 28)	IPAF (n = 20)
Male sex, n (%)	19 (95.0)	8 (53.3)	10 (35.7)	10 (50.0)
Age (yr), mean (range)	66.0 (58–79)	58.1 (37–71)	55.8 (34–68)	56.8 (37–80)
Drugs, n (%)				
Nintedanib	2 (10)	1 (6.7)	1 (3.6)	1 (5)
Pirfenidone	16 (80)	12 (80)	24 (85.7)	16 (80)
Imatinib	0	1 (6.7)	0	1 (5)
FAPI SUVmean, mean (range)	2.5 (2.3–2.8)	2.3 (2.2–2.5)	2.5 (2.1–3.3)	2.5 (2.1–2.8)
FAPI SUV total (g/ml·cm³), mean (range)	1,010.3 (83.2–2,393.6)	375.0 (14.8–1,200.2)	468.5 (8.8–2,044.4)	468.8 (2.4–1,445.3)
KL-6 (U/ml), mean (range)	1,391.7 (480–4,949)	1,425.3 (369–4,561)	1,942.8 (408–5,162)	1,556.8 (448–4,192)
Baseline FVC (% predicted), mean (range)	80.0 (54.0–106.8)	78.9 (40.3–109.7)	68.8 (32.6–103.4)	71.9 (50.0–98.8)
Baseline $D_{L_{CO}}$ (% predicted), mean (range)	37.6 (17.0–58.3)	55.2 (24.3–79.6)	47.2 (30.6–68.8)	48.3 (26.1–73.6)

Definition of abbreviations: CTD = connective tissue disease; IPAF = interstitial pneumonia with autoimmune features; IPF = idiopathic pulmonary fibrosis; KL-6 = Krebs von den lungen-6; NSIP = nonspecific interstitial pneumonitis; SUV = standard uptake value.
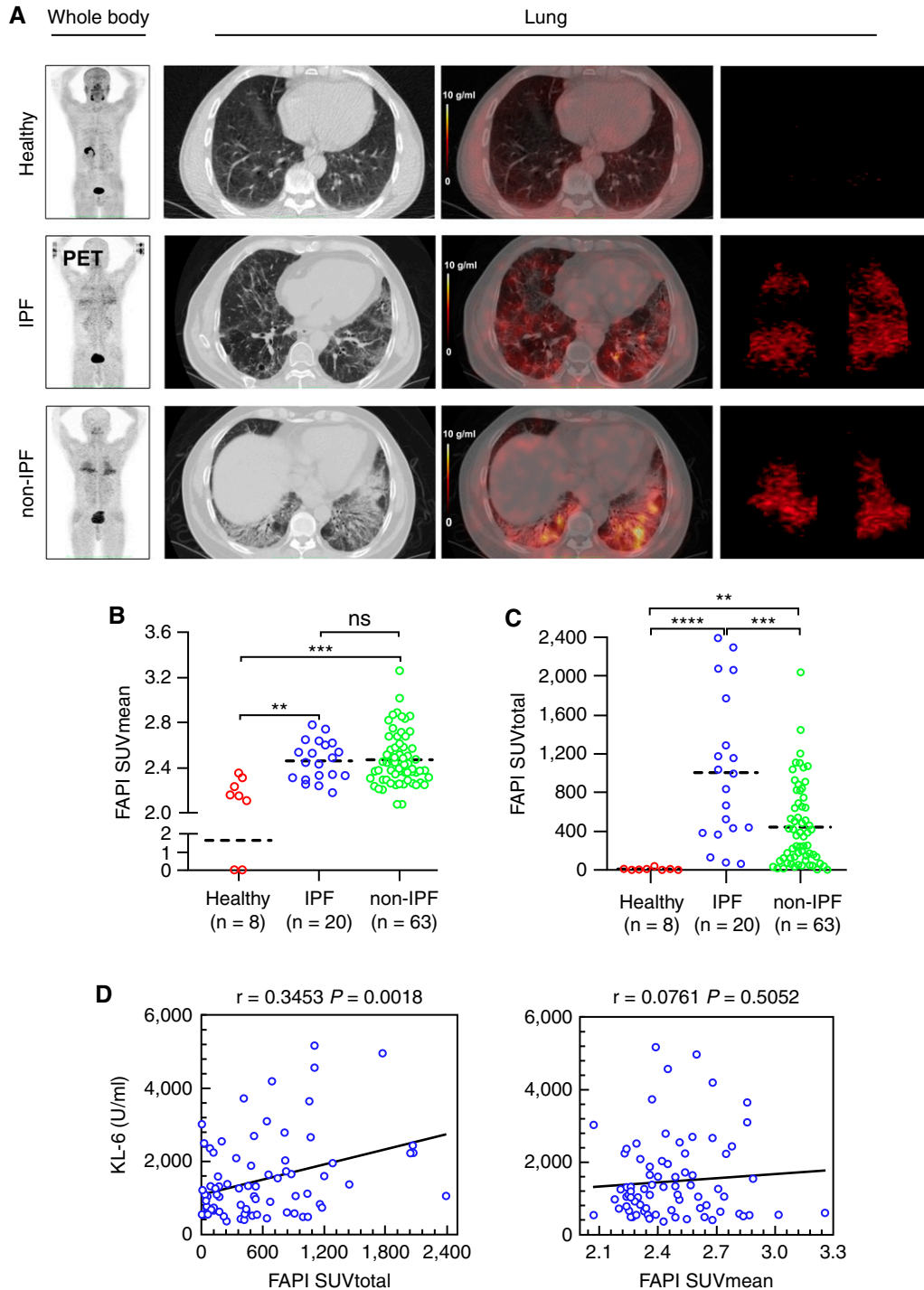
Figure 5. Fibroblast activation protein (FAP)-targeted positron emission tomography (PET)/computed tomography (CT) imaging of patients with interstitial lung disease (ILD). A total of 78 patients diagnosed as idiopathic pulmonary fibrosis (IPF) ($n = 20$), non-IPF ILD ($n = 63$), and healthy volunteers ($n = 8$) were recruited for a PET imaging study with ^{68}Ga-FAPI-04. (A) The columns from left to right successively showed representative images of whole-body uptake for ^{68}Ga-FAPI-04 with PET, ^{68}Ga-FAPI-04 uptake in lung cross-section with CT, PET/CT, and the ^{68}Ga-FAPI-04 total uptake with PET by three-dimensional (3-D) reconstruction. (B) Mean of standard uptake value (SUVmean) for ^{68}Ga-FAPI-04 in all patients with ILD and healthy volunteers. The dashed line is a median. ****$P < 0.0001$. (C) Quantitative analysis for total volume uptake of PET tracer targeting FAP (SUVtotal) in different subtypes of patients with ILD and healthy volunteers. The dashed line is a median. **$P < 0.01$, ***$P < 0.001$, and ****$P < 0.0001$. (D) Correlation analysis between the uptake of ^{68}Ga-FAPI-04 (SUVmean and SUVtotal) in ILDs (including patients with and without IPF) with KL-6, linear regression (r), and linear regression lines are plotted. $P < 0.05$ was considered statistically significant. ns = no significance.
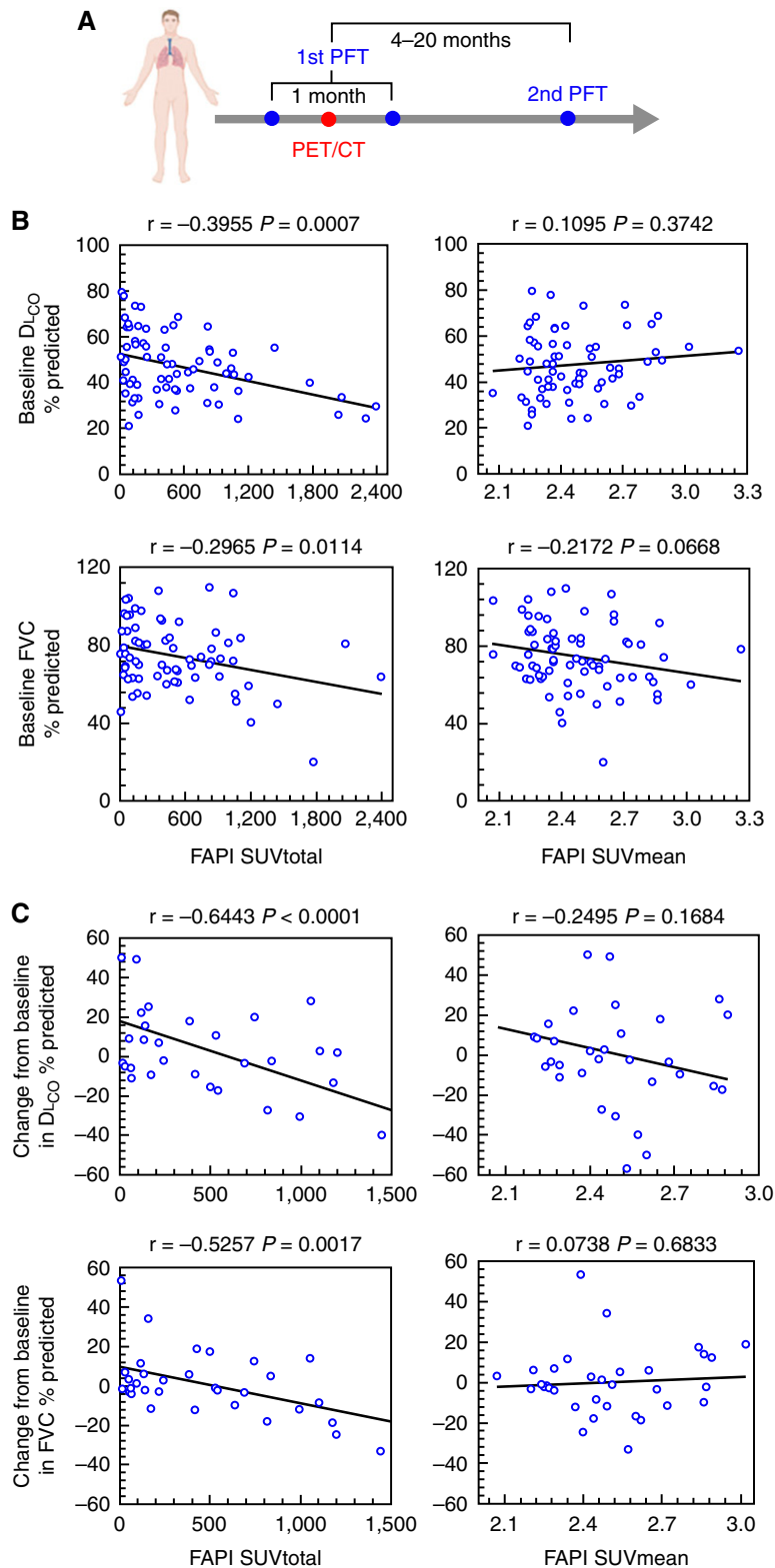
Figure 6. Correlation analysis for ^{68}Ga-FAPI-04 uptake and pulmonary function test (PFT). (*A*) Timeline for positron emission tomography (PET)/computed tomography (CT) and PFT: the first PFT was conducted within no more than 1 month from PET/CT scan. The time interval between the two PFT measurements was approximately 4–20 months. (*B*) Correlation analysis between standard uptake value (SUV) for ^{68}Ga-FAPI-04 (SUVtotal and SUVmean) and PFT (baseline D_{LCO} and FVC). (*C*) Correlation analysis between ^{68}Ga-FAPI-04 (SUVtotal and SUVmean) uptake and changes in PFT (change from baseline in D_{LCO} and FVC). Linear regression (*r*) and linear regression lines are plotted. *P* < 0.05 was considered statistically significant. FAPI = fibroblast activation protein inhibitors.

SUVmean, whereas they were significantly negatively associated with the SUVtotal (Figures 6B and 6C). In addition, PFT alterations showed a much higher correlation to SUVtotal than baseline PFT did ($\Delta D_{L_{CO}}$% predicted: $r = -0.6443$, $P < 0.0001$; baseline $D_{L_{CO}}$% predicted: $r = -0.3955$, $P = 0.0007$; ΔFVC% predicted: $r = -0.5257$, $P = 0.0017$; baseline FVC% predicted: $r = -0.2965$, $P = 0.0114$).

Altogether, it could be concluded that FAP-targeted PET/CT imaging could be reliably used to noninvasively monitor the abundance and distribution of activated fibroblasts in various types of ILDs, and the SUVtotal of PET/CT tracer could reflect the severity of ILD.

Discussion

This current study provided cellular, pathological, and imaging profiles of FAP in ILDs. These preclinical and clinical data collectively imply that FAP might act as a universal and reliable biomarker to *in situ* report the fibrotic activity of any subtype of ILDs.

One of the notable findings from the present work was that low-dose TGF-β could pronouncedly induce FAP protein in primary lung fibroblasts from 24 hours after treatment. In sharp contrast, the expression of both α-SMA and fibronectin seemed to occur relatively late and required a high concentration of TGF-β. These unique expression profiles hint that FAP might be superior to those conventional fibrosis markers in prewarning the advent of fibrotic events, which may be valuable to early diagnostics.

Although a previous study reported that FAP expression could be detected in a minor subpopulation of M2 macrophages in tumors (37), we analyzed the public data from single-cell seq data showing that nearly all FAP-positive cells in ILD lungs were fibroblasts. Moreover, the relative expression levels between *FAP* and other fibrosis markers in ILDs, such as *ACTA2*, *COL1A1*, and *FN1*, were highly correlated. The high cell-type specificity of FAP in ILD lungs suggests that it might be particularly suitable to be used as a biomarker to accurately describe the position and abundance of active fibroblasts under *in vivo* circumstances.

Several previous studies have tried to use specific PET radioactive probes to mark the position and extent of fibrosis. The corresponding targets include collagens and their degradation products (38, 39), triggers of profibrotic cytokine activation, and modulators of cell phenotype (40, 41). Unlike these biomarkers, which can only indirectly reflect the initiation or history of fibrotic reactions, FAP may represent a promising clinically feasible biomarker to quantitatively report ongoing fibrosis because it is a membrane-anchored protein in active fibroblasts.

Another major finding is that the amounts of FAP-expressing cells reflected by either immunostaining or PET/CT images sharply varied in different ILD individuals. Immunostaining assay only shows FAP expression status in a certain section of one part of the lesion area, which is highly dependent on lung biopsy location. PET/CT imaging provides FAP-positive signals within the entire lung. The patients with many lung FAP-positive cells may be at the active fibrosis stage, and others that are negative for FAP may be at relatively stable fibrosis. This speculation can be partially supported by the patients' PFT changes and are in accord with the fact that the fibrotic reaction in ILDs is not always active (42). Hence, the *in vivo* determination of FAP status may benefit ILD diagnosis in at least two aspects. First, the actively fibrotic phase might be noninvasively evaluated so early intervention with antifibrotic drugs can be conducted. Second, those patients with resting late ILD could also be discriminated from their active counterparts to avoid previous blind prescriptions of antifibrotic agents because of drug-induced side effects (43).

The current PET study indicated that the distribution pattern of FAP-positive cells in IPF lungs tended to be rather scattered, opposite to an aggregated mode observed in the non-IPF group. Therefore, it is easy to understand that patient disease severity, reflected by either serum concentration of KL-6 or lung function decline, demonstrated a significant negative correlation with the total uptake of ^{68}Ga-FAPI tracer in the lung rather than the SUVmean. To our knowledge, this is the first study to compare the distribution of active fibroblasts in IPF with non-IPF ILDs. The gradually accepted concept might partially explain this phenomenon that aging is an important etiology for IPF (44), making it reasonable that aging-induced injury scope was supposed to be pervasive rather than local.

As for the correlation between the abundance of FAP-expressing cells in the lung with the disease outcome, our study demonstrated that those patients with more uptake of FAPI tracer tended to exhibit a rapid lung function decline after the PET scan, albeit they have all received treatment with antifibrotic drugs. In contrast, those patients with less PET tracer uptake showed decreased damage in lung function. These results strongly imply that the number of FAP-positive cells can serve as an important index to predict treatment response or lung function changes. A further prospective study in a larger cohort is needed to confirm this clinically important finding.

We also found that the FAP abundance in ILD lungs was positively associated with patient serum concentrations of KL-6. Even though the KL-6 concentration is highly correlated with epithelial injury and the severity of lining fibrosis (45), a recent randomized controlled trial reported that it could not predict the patient response to therapy with antifibrotic drugs (46). Because most current compounds targeting fibrosis were developed to attenuate the process of fibroblast activation, an event taking place downstream of alveolar injury, it becomes easy to understand why KL-6 produced by the damaged lung epithelium failed to assess the therapeutic effects. According to this logic, approaches to monitor FAP might be an ideal short-term readout for the drug's antifibrotic activity that all the researchers in the field of ILDs have been expecting because it directly detects the effector cells of fibrosis (42).

Conclusions
Conventional diagnostic methods influencing the decision to treat include radiology assessment of ILD severity and lung function testing. Because these structural and functional demonstrations lag behind the occurrence of activated fibroblasts, it can be envisaged that FAP-targeted noninvasive imaging might potentially predict the outbreak of fibrotic reactions with high sensitivity and allow for early intervention. ∎

References

1. Rockey DC, Bell PD, Hill JA. Fibrosis–0a common pathway to organ injury and failure. *N Engl J Med* 2015;372:1138–1149.
2. Jun JI, Lau LF. Resolution of organ fibrosis. *J Clin Invest* 2018;128:97–107.
3. Ryu JH, Moua T, Daniels CE, Hartman TE, Yi ES, Utz JP, *et al.* Idiopathic pulmonary fibrosis: evolving concepts. *Mayo Clin Proc* 2014;89:1130–1142.
4. Richeldi L, Collard HR, Jones MG. Idiopathic pulmonary fibrosis. *Lancet* 2017;389:1941–1952.
5. Barratt SL, Creamer A, Hayton C, Chaudhuri N. Idiopathic pulmonary fibrosis (IPF): an overview. *J Clin Med* 2018;7:201.
6. Ebner L, Christodoulidis S, Stathopoulou T, Geiser T, Stalder O, Limacher A, *et al.* Meta-analysis of the radiological and clinical features of usual interstitial pneumonia (UIP) and nonspecific interstitial pneumonia (NSIP). *PLoS One* 2020;15:e0226084.
7. Sheth JS, Belperio JA, Fishbein MC, Kazerooni EA, Lagstein A, Murray S, *et al.* Utility of transbronchial vs surgical lung biopsy in the diagnosis of suspected fibrotic interstitial lung disease. *Chest* 2017;151:389–399.
8. Cottin V. Lung biopsy in interstitial lung disease: balancing the risk of surgery and diagnostic uncertainty. *Eur Respir J* 2016;48:1274–1277.
9. Fitzgerald AA, Weiner LM. The role of fibroblast activation protein in health and malignancy. *Cancer Metastasis Rev* 2020;39:783–803.
10. Puré E, Blomberg R. Pro-tumorigenic roles of fibroblast activation protein in cancer: back to the basics. *Oncogene* 2018;37:4343–4357.
11. Attieh Y, Vignjevic DM. The hallmarks of CAFs in cancer invasion. *Eur J Cell Biol* 2016;95:493–502.
12. Park JE, Lenter MC, Zimmermann RN, Garin-Chesa P, Old LJ, Rettig WJ. Fibroblast activation protein, a dual specificity serine protease expressed in reactive human tumor stromal fibroblasts. *J Biol Chem* 1999;274: 36505–36512.
13. Scanlan MJ, Raj BK, Calvo B, Garin-Chesa P, Sanz-Moncasi MP, Healey JH, *et al.* Molecular cloning of fibroblast activation protein alpha, a member of the serine protease family selectively expressed in stromal fibroblasts of epithelial cancers. *Proc Natl Acad Sci USA* 1994;91: 5657–5661.
14. Dorst DN, Rijpkema M, Boss M, Walgreen B, Helsen MMA, Bos DL, *et al.* Targeted photodynamic therapy selectively kills activated fibroblasts in experimental arthritis. *Rheumatology (Oxford)* 2020;59:3952–3960.
15. Wäldele S, Koers-Wunrau C, Beckmann D, Korb-Pap A, Wehmeyer C, Pap T, *et al.* Deficiency of fibroblast activation protein alpha ameliorates cartilage destruction in inflammatory destructive arthritis. *Arthritis Res Ther* 2015;17:12.
16. Acharya PS, Zukas A, Chandan V, Katzenstein AL, Puré E. Fibroblast activation protein: a serine protease expressed at the remodeling interface in idiopathic pulmonary fibrosis. *Hum Pathol* 2006;37:352–360.
17. Aghajanian H, Kimura T, Rurik JG, Hancock AS, Leibowitz MS, Li L, *et al.* Targeting cardiac fibrosis with engineered T cells. *Nature* 2019;573: 430–433.
18. Meletta R, Müller Herde A, Chiotellis A, Isa M, Rancic Z, Borel N, *et al.* Evaluation of the radiolabeled boronic acid-based FAP inhibitor MIP-1232 for atherosclerotic plaque imaging. *Molecules* 2015;20:2081–2099.
19. Rurik JG, Tombácz I, Yadegari A, Méndez Fernández PO, Shewale SV, Li L, *et al.* CAR T cells produced in vivo to treat cardiac injury. *Science* 2022;375:91–96.
20. Jansen K, Heirbaut L, Cheng JD, Joossens J, Ryabtsova O, Cos P, *et al.* Selective inhibitors of fibroblast activation protein (FAP) with a (4-Quinolinoyl)-glycyl-2-cyanopyrrolidine scaffold. *ACS Med Chem Lett* 2013;4:491–496.
21. Jansen K, Heirbaut L, Verkerk R, Cheng JD, Joossens J, Cos P, *et al.* Extended structure-activity relationship and pharmacokinetic investigation of (4-quinolinoyl)glycyl-2-cyanopyrrolidine inhibitors of fibroblast activation protein (FAP). *J Med Chem* 2014;57:3053–3074.
22. Kratochwil C, Flechsig P, Lindner T, Abderrahim L, Altmann A, Mier W, *et al.* 68Ga-FAPI PET/CT: tracer uptake in 28 different kinds of cancer. *J Nucl Med* 2019;60:801–805.
23. Luo Y, Pan Q, Yang H, Peng L, Zhang W, Li F. Fibroblast activation protein-targeted PET/CT with 68Ga-FAPI for imaging IgG4-related disease: comparison to 18F-FDG PET/CT. *J Nucl Med* 2021;62:266–271.
24. Carvajal Alegria G, Croft AP. Fibroblasts, a target for imaging and therapeutics in rheumatoid arthritis. *Rheumatology (Oxford)* 2021;61: 2726–2727.
25. Altmann A, Haberkorn U, Siveke J. The latest developments in imaging of fibroblast activation protein. *J Nucl Med* 2021;62:160–167.
26. Fan MH, Zhu Q, Li HH, Ra HJ, Majumdar S, Gulick DL, *et al.* Fibroblast activation protein (FAP) accelerates collagen degradation and clearance from lungs in mice. *J Biol Chem* 2016;291: 8070–8089.
27. Kimura T, Monslow J, Klampatsa A, Leibowitz M, Sun J, Liousia M, *et al.* Loss of cells expressing fibroblast activation protein has variable effects in models of TGF-β and chronic bleomycin-induced fibrosis. *Am J Physiol Lung Cell Mol Physiol* 2019;317:L271–L282.
28. Loktev A, Lindner T, Burger EM, Altmann A, Giesel F, Kratochwil C, *et al.* Development of fibroblast activation protein-targeted radiotracers with improved tumor retention. *J Nucl Med* 2019;60:1421–1429.
29. Bian H, Nie X, Bu X, Tian F, Yao L, Chen J, *et al.* The pronounced high expression of discoidin domain receptor 2 in human interstitial lung diseases. *ERJ Open Res* 2018;4:00138-2106.
30. Stritt M, Stalder AK, Vezzali E. Orbit image analysis: an open-source whole slide image analysis tool. *PLOS Comput Biol* 2020;16:e1007313.
31. Saito A, Horie M, Nagase T. TGF-β signaling in lung health and disease. *Int J Mol Sci* 2018;19:2460.
32. Wu G, Xie B, Lu C, Chen C, Zhou J, Deng Z. microRNA-30a attenuates TGF-β1-induced activation of pulmonary fibroblast cell by targeting FAP-α. *J Cell Mol Med* 2020;24:3745–3750.
33. Chen H, Yang WW, Wen QT, Xu L, Chen M. TGF-beta induces fibroblast activation protein expression; fibroblast activation protein expression increases the proliferation, adhesion, and migration of HO-8910PM [corrected]. *Exp Mol Pathol* 2009;87:189–194.
34. Zhang H, Chen L, Wu L, Huang J, Li H, Wang X, *et al.* Diagnostic and prognostic predictive values of circulating KL-6 for interstitial lung disease: a PRISMA-compliant systematic review and meta-analysis. *Medicine (Baltimore)* 2020;99:e19493.
35. Caron M, Hoa S, Hudson M, Schwartzman K, Steele R. Pulmonary function tests as outcomes for systemic sclerosis interstitial lung disease. *Eur Respir Rev* 2018;27:170102.
36. Cameli P, Bargagli E, Bergantini L, Refini RM, Pieroni M, Sestini P, *et al.* Evaluation of multiple-flows exhaled nitric oxide in idiopathic and non-idiopathic interstitial lung disease. *J Breath Res* 2019;13: 026008.
37. Arnold JN, Magiera L, Kraman M, Fearon DT. Tumoral immune suppression by macrophages expressing fibroblast activation protein-α and heme oxygenase-1. *Cancer Immunol Res* 2014;2:121–126.
38. Wallace WE, Gupta NC, Hubbs AF, Mazza SM, Bishop HA, Keane MJ, *et al.* Cis-4-[(18)F]fluoro-L-proline PET imaging of pulmonary fibrosis in a rabbit model. *J Nucl Med* 2002;43:413–420.
39. Désogère P, Tapias LF, Hariri LP, Rotile NJ, Rietz TA, Probst CK, *et al.* Type I collagen-targeted PET probe for pulmonary fibrosis detection and staging in preclinical models. *Sci Transl Med* 2017;9: eaaf4696.
40. Kimura RH, Wang L, Shen B, Huo L, Tummers W, Filipp FV, *et al.* Evaluation of integrin αvβ6 cystine knot PET tracers to detect cancer and idiopathic pulmonary fibrosis. *Nat Commun* 2019;10:4673.
41. Withana NP, Ma X, McGuire HM, Verdoes M, van der Linden WA, Ofori LO, *et al.* Non-invasive imaging of idiopathic pulmonary fibrosis using cathepsin protease probes. *Sci Rep* 2016;6:19755.
42. Spagnolo P, Maher TM. Clinical trial research in focus: why do so many clinical trials fail in IPF? *Lancet Respir Med* 2017;5:372–374.
43. Mikolasch TA, Garthwaite HS, Porter JC. Update in diagnosis and management of interstitial lung disease. *Clin Med (Lond)* 2017;17: 146–153.
44. Zank DC, Bueno M, Mora AL, Rojas M. Idiopathic pulmonary fibrosis: aging, mitochondrial dysfunction, and cellular bioenergetics. *Front Med (Lausanne)* 2018;5:10.
45. d'Alessandro M, Bergantini L, Cameli P, Vietri L, Lanzarone N, Alonzi V, *et al.* Krebs von den Lungen-6 as a biomarker for disease severity assessment in interstitial lung disease: a comprehensive review. *Biomarkers Med* 2020;14:665–674.
46. Maher TM, Stowasser S, Nishioka Y, White ES, Cottin V, Noth I, *et al.*; INMARK trial investigators. Biomarkers of extracellular matrix turnover in patients with idiopathic pulmonary fibrosis given nintedanib (INMARK study): a randomised, placebo-controlled study. *Lancet Respir Med* 2019;7:771–779.